

# Influence of layer roughness for road survey by ground penetrating radar at nadir: theoretical study

N. Pinel<sup>1</sup> C. Le Bastard<sup>2</sup> V. Baltazart<sup>3</sup> C. Bourlier<sup>1</sup> Y. Wang<sup>1</sup>

<sup>1</sup>IREENA (Institut de Recherche en Electrotechnique et Electronique de Nantes Atlantique) Laboratory, Université Nantes Angers Le Mans, Polytech'Nantes, La Chantrerie, rue C. Pauc, BP 50609, 44306 Nantes Cedex 3, France

<sup>2</sup>Laboratoire Régional des Ponts et Chaussées d'Angers, 23 avenue de l'Amiral Chauvin, BP 69, 49136 Les Ponts de Cé, France

<sup>3</sup>Laboratoire Central des Ponts et Chaussées, BP 4129, 44341 Bouguenais Cedex, France  
E-mail: nicolas.pinel@univ-nantes.fr

**Abstract:** In civil engineering, conventional methods used to estimate the thickness of pavements assume flat interfaces. In contrast, this study uses a rigorous electromagnetic method called propagation-inside-layer-expansion (PILE) to simulate the radar backscattered signal at nadir from a rough pavement made up of two rough interfaces separating homogeneous media. The statistical distribution of the first two echoes is studied by comparison with the default flat case, together with their frequency behaviour. Within the scope of road pavement survey by ground penetrating radar, the scattering model is finally used to assess the performance of the estimation of signal parameters via rotational invariance techniques (ESPRIT) algorithm, one of the well-known high-resolution time-delay estimation techniques.

## 1 Introduction

Ground penetrating radar (GPR) is a common tool for non-destructive probing of civil engineering materials (hydraulic and bituminous concretes, soils). For centimetre-scale wavelengths, GPR is often used for the specific application of pavement survey [1, 2]. For this purpose, the roadway is assumed to be horizontally stratified. The vertical structure of the roadway can then be deduced from radar profiles by means of echo detection and estimation of amplitudes. Echo detection provides the time-delay estimation (TDE) associated with each interface, whereas amplitude estimation is used to retrieve the wave speed within each layer. Some particular pavement materials are made up of thin layers (having thicknesses <3 cm), which requires the use of high-resolution algorithms for thickness estimation [1, 2].

Conventional signal processing techniques that are used to perform thickness estimation neglect both surface and volume scattering. The heterogeneity of the pavement material (made up of aggregates of 2 cm at the most) may contribute to the overall scattering, and may consequently lead to additional errors in the thickness estimation. However, according to [3], at nadir and within the GPR band, surface scattering dominates in comparison with volume scattering. Thus, this paper focuses on the influence of the roughness of the surfaces on the electromagnetic wave scattering from the stratified pavement. Compared to [4, 5] in which only a single rough interface is considered, this requires much more sophisticated electromagnetic modelling. A rigorous approach named PILE (propagation-inside-layer-expansion) method [6] is then used. The solution is then expected to

bring a better insight in the scattering phenomena: to determine the validity domain of the flat interface assumption and to assess the performance of the thickness estimation technique.

This paper is organised as follows. In Section 2, the PILE method [6] rigorously calculates the backscattered echoes by the rough stratified pavement. Each rough interface is characterised by a Gaussian distribution and an exponential auto-correlation. The results are compared with the standard case of flat interfaces. Owing to the limited extent of the illumination beam, a spatial variability of the backscattered echoes occurs, depending on the location of the measurement. Thus, this variability is theoretically studied by computing the statistical distribution of the backscattered echoes. The frequency signature of the echoes within studied frequency band (with bandwidth  $B = 3$  GHz and centre frequency  $f_c = 2$  GHz) is shown to depend on the roughness of the interfaces. Then, the simulated electromagnetic data are used to assess the performance of the selected time-delay processing for pavement survey by GPR, with regard to the signal-to-noise ratio (SNR). The selected TDE technique, namely ESPRIT (estimation of signal parameters via rotational invariance techniques) technique, is presented in Section 3. It was selected among the subspace algorithms family (MUSIC, Min Norm) because of its smaller computational burden. The principle of this algorithm is briefly recalled, as well as the associated assumptions in the signal model. In Section 4, computer tests show the influence of the layer roughness on the performances of the ESPRIT algorithm.

## 2 Rough pavement scattering modelling

This section details the influence of the surface roughness of the stratified pavement on the scattered echoes, as illustrated in Fig. 1. Analytical formulas based on the Rayleigh roughness parameter allow us a qualitative analysis of the latter influence. Then, the numerical method PILE [6] is used to obtain quantitative results. In comparison with the literature, the PILE method aims at improving the realism of simulated data. The simulated data match the conventional radar configuration used for road survey by GPR (e.g. [7–9]), that is, monostatic radar backscattered data at nadir.

### 2.1 Qualitative analysis

In this subsection, the influence of surface roughness is examined from a qualitative point of view for the problem configuration shown in Fig. 1 considering only two interfaces.

First, the simple case of a flat layer (with two flat interfaces) of thickness  $\bar{H}$  is considered. For normal incidence  $\theta_i = 0$  (nadir), the first and second echoes  $s_1$  and  $s_2$  (corresponding to scattered fields  $E_1$  and  $E_2$  in Fig. 1) backscattered (i.e. specular reflection) by the two (flat) surfaces of the pavement ( $\Sigma_A$  and  $\Sigma_B$ , respectively) are given by

$$s_1 = \frac{E_1}{E_i} = r_{12} \quad (1)$$

$$s_2 = \frac{E_2}{E_i} = t_{12}r_{23}t_{21}e^{-2\bar{H}k_0\Im m(\sqrt{\epsilon_{r2}})} \quad (2)$$

respectively, with  $r_{12}$  and  $r_{23}$  the Fresnel reflection coefficients at the upper and lower (flat) surfaces  $\Sigma_A$  and  $\Sigma_B$ , respectively, and  $E_i$  the incident field. In addition to  $r_{23}$ , the second echo  $s_2$  takes account of Fresnel transmission coefficients  $t_{12}$  and  $t_{21}$  through the upper flat surface  $\Sigma_A$ , and an additional term owing to the propagation loss inside the lossy pavement layer  $\Omega_2$ .

Here,  $s_2$  is defined regardless of the real part of phase difference between  $E_1$  and  $E_2$ ,  $2\bar{H}k_0\Re e(\sqrt{\epsilon_{r2}})$ , which will be taken into account when studying TDE, see the term  $e^{-2j\pi T/k}$  in (7).  $k_0$  is the wavenumber inside the vacuum,  $\epsilon_{r2}$  the complex relative permittivity of inner medium  $\Omega_2$  and  $\Im m$  the imaginary part operator.

Second, compared with the latter case of two flat surfaces, the surface roughness induces a broadening of the energy away from nadir  $\theta_s = \theta_i = 0$ . As a result, the backscattered echoes  $s_1$  and  $s_2$  are expected to decrease in amplitude, depending on the RMS (root mean square) height of the rough surfaces with respect to the electromagnetic wavelength in the vacuum  $\lambda_0$ .

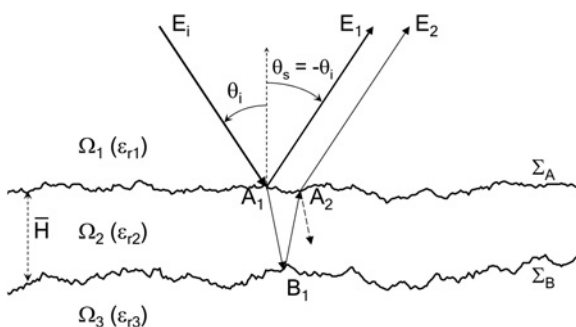


Fig. 1 Problem configuration (for the illustration, the incidence is oblique:  $\theta_i \neq 0$ )

The typical surface RMS height is of the order of 1 mm [5, 10], whereas the wavelength in the vacuum  $\lambda_0$  ranges from 0.600 to 0.086 m for a GPR frequency band ranging from 0.5 to 3.5 GHz. Therefore the modification of the echo levels  $s_k = E_k/E_i$  owing to the surface roughness is expected to be rather small, and in particular for  $s_1$ .

Then, to further study the influence of interlayer surface roughness on the echo amplitudes, the Rayleigh roughness parameter  $Ra$ , which is well known for the case of reflection from single rough interfaces [11], is used, and its associated Fraunhofer criterion [12] is introduced. Considering the reflection onto the upper interface  $\Sigma_A$ , it is usually given for normal incidence  $\theta_i = 0$  by the relation [11, 13]

$$Ra_{r,1} = k_0 n_1 \sigma_{hA} \quad (3)$$

with  $n_1 = 1$  the refractive index of  $\Omega_1$  and  $\sigma_{hA}$  the RMS height of  $\Sigma_A$ . Equation (3) corresponds to the Rayleigh roughness parameter associated with the scattered field  $E_1$  (see Fig. 1).

Recent work [13, 14] made it possible to extend the Rayleigh roughness parameter  $Ra$  to the case of reflection from a rough layer. For a Gaussian process (i.e. for rough surfaces with Gaussian height PDF, probability density function), a satisfactory agreement was found in [13, 15] between the extended Rayleigh roughness parameters and exact numerical results. Then, this new tool provides us an interesting means to evaluate the electromagnetic roughness of rough layers. For uncorrelated rough surfaces, the extended Rayleigh roughness parameter  $Ra_{r,2}$  associated with the second-order scattered field  $E_2$  (or associated second echo  $s_2$ ) is given for normal incidence  $\theta_i = 0$  and lossless media  $\Omega_1$  and  $\Omega_2$  by [13, 15]

$$Ra_{r,2} = \sqrt{2k_0^2 \sigma_{hA}^2 \frac{|n_1 - n_2|^2}{4} + k_2^2 \sigma_{hB}^2} \quad (4)$$

where  $n_2$  is the refractive index of  $\Omega_2$  and  $\sigma_{hB}$  the RMS height of  $\Sigma_B$ .

A qualitative criterion (associated to the Rayleigh roughness parameter) can be used to check if the surface or layer can be considered as slightly rough. Called Fraunhofer criterion, it is given by [12]

$$Ra < \pi/16 \simeq 0.196 \quad (5)$$

Here, for electromagnetic probing of rough pavements (with millimetre-scale surface RMS heights) at decimetre-scale microwave frequencies, the first-order Rayleigh parameter  $Ra_{r,1}$ , given by (3), is very weak and checks the Fraunhofer criterion. This means that for  $s_1$ , the layer can be considered as very slightly rough. Nevertheless, the second-order Rayleigh parameter  $Ra_{r,2}$  associated with  $s_2$ , given by (4), is  $> Ra_{r,1}$ , and can exceed the Fraunhofer limit,  $\pi/16$ . In particular, we will see hereafter that it is true for the higher frequencies of the GPR band: in the example to follow, it is reached at  $f \simeq 2.17$  GHz. This means that for  $s_2$ , the layer can be considered as either slightly rough or rough electromagnetically.

Similarly as in [4], because the pavement area illuminated by the GPR antenna is not much larger than the upper and lower surface correlation lengths  $L_{cA}$  and  $L_{cB}$ , respectively, a variability of the backscattered echoes occurs, depending on

the location of the measurement. Thus, hereafter this variability is studied theoretically by computing the statistical distribution (also called probability density function, PDF) of the backscattered echoes. Then, the frequency behaviour of the echoes is studied within considered frequency band.

In what follows, a quantitative analysis is led by means of a rigorous numerical method, in order to validate the qualitative analysis and to study more precisely the surface roughness influence on the electromagnetic scattering.

## 2.2 Quantitative analysis

In order to compute the fields scattered from the rough layer, a numerical method, based on the method of moments (MoM), is used. This method, called the PILE method [6], is a rigorous numerical method.

Contrary to other MoM-based reference numerical methods that generally can calculate only the total scattered field from rough layers  $E_{tot} = \sum_{k=1}^{\infty} E_k = E_1 + E_2 + \dots$ , the PILE method is able to rigorously compute each scattered field contribution ( $E_1$ ,  $E_2$ , and so on, see Fig. 1). Therefore this method is appropriate for the computation of the different echoes  $s_k = E_k/E_i$  (see (2) of [2]), instead of considering the simple case of flat interfaces. Thus, numerical simulations are led to derive  $s_k$ .

## 2.3 Simulation parameters

The simulation parameters are chosen to match to the conventional GPR configuration used for pavement survey at traffic speed (e.g. [9]), that is, air-coupled radar configuration at vertical incidence (nadir). It is assumed that the scope of the probing is limited to the first two layers of the pavement structure.

Studied pavement structure is made up of a layer medium  $\Omega_2$  of ultra thin asphalt surfacing (UTAS) of mean thickness  $\bar{H} = 20$  mm [16], overlying a rolling band  $\Omega_3$  of same general composition (see Fig. 1). The UTAS and the rolling band are assumed to be equivalent to homogeneous media at normal incidence and at the frequency band under study  $f \in [0.5; 3.5]$  GHz [2, 3, 7]. Their relative permittivities  $\epsilon_r$  typically range between 4 and 8 [17, 18], and their conductivities  $\sigma$  between  $10^{-3}$  and  $10^{-2}$  S/m [8]. For the simulations, we take  $\epsilon_{r2} = 4.5$  and  $\epsilon_{r3} = 7$ , respectively, and  $\sigma_2 = 5 \times 10^{-3}$  S/m and  $\sigma_3 = 10^{-2}$  S/m, respectively. Then, by considering non-dispersive media, the complex relative permittivity  $\underline{\epsilon}_r$  can be calculated as

$$\underline{\epsilon}_r = \epsilon_r + j \frac{\sigma}{2\pi f \epsilon_0} \quad (6)$$

with  $\epsilon_0 = 10^{-9}/36\pi$  F/m the permittivity inside the vacuum. For instance, for  $f = 2$  GHz, the complex relative permittivities are  $\underline{\epsilon}_{r2} = 4.5 + j0.045$  and  $\underline{\epsilon}_{r3} = 7 + j0.090$ . The two rough interfaces  $\Sigma_A$  and  $\Sigma_B$  are assumed to have a Gaussian height PDF and an exponential height auto-correlation function [5, 10]. For  $\Sigma_A$ , the RMS height  $\sigma_{hA}$  is of the order of 0.6–1 mm, and the correlation length  $L_{cA}$  of the order of 5–10 mm [5, 10]. For  $\Sigma_B$ , the RMS height  $\sigma_{hB}$  and the correlation length  $L_{cB}$  are a bit greater. Chosen simulation parameters are  $\sigma_{hA} = 1.0$  mm,  $L_{cA} = 6.4$  mm,  $\sigma_{hB} = 2.0$  mm and  $L_{cB} = 15.0$  mm. In practice, the two rough surfaces are only weakly correlated; thus, the height profiles of the two surfaces have been generated from independent processes for the data sets.

The antenna is assumed to radiate a vertically polarised plane wave in far field of probed pavement as in [19]: the antenna is about 400 mm above the sand surface, for which far-field condition has been checked from data. The antenna is thus located beyond the Fraunhofer distance with respect to the probed pavement. This air-coupled radar configuration allows us to implement the advanced signal processing technique to be introduced in Section 3 for TDE.

The typical width of probed surface antenna footprint is of the order of 300–500 mm [19, 20]. Then, for the simulations, surfaces of length  $L = 2400$  mm are considered, illuminated by a Thorsos beam of attenuation parameter  $g = L/6$  [21] (the Thorsos beam is a tapered plane wave, whose tapering has a Gaussian shape; the tapering is used to reduce the incident field to near zero at the ends of the surface realisations and thereby to reduce edge effects to negligible levels). The two rough interfaces are sampled with a sampling step  $\Delta x = \lambda_2/10$ , with  $\lambda_2$  the wavelength inside  $\Omega_2$ . A normal ( $\theta_i = 0$ ) incident wave is taken, and the first two orders of the reflected fields by the rough layer  $E_1$  and  $E_2$  are calculated under the PILE method, in order to derive the first two echoes  $s_1$  and  $s_2$  from the ratios  $s_1 = E_1/E_i$  and  $s_2 = E_2/E_i$ . Then, the frequency signature of the two echoes  $s_k \equiv s_k(f)$  are obtained by running the PILE code at the different frequencies  $f$  over the GPR band, that is, [0.5; 3.5] GHz.

To study the variability of the echo amplitudes  $s_1$  and  $s_2$  (which occurs because the antenna footprint (or spot size) is not much larger than  $L_{cA}$  and  $L_{cB}$ , as often in pavement measurement processes [4]), several independent Monte-Carlo processes are generated. Thus, it is possible to estimate the standard deviations of the echo amplitudes, and even a profile of their calculated PDFs if a significant number of realisations is used (typically, of the order of  $N = 10\,000$  [22]). In what follows, a great number of realisations is then used to thoroughly study the influence of the variability of the surface roughnesses on the echoes.

## 2.4 Numerical results

First, numerical simulations are led at a fixed radar frequency  $f$ , in the centre of studied radar band, that is,  $f = f_c = 2.0$  GHz. In order to study the PDF of the echoes  $s_1$  and  $s_2$ , we take  $N = 10\,000$  realisations of the Monte-Carlo process. A comparison is also made with the case of flat interfaces (in green vertical line). Numerical results of computed PDFs are plotted in Fig. 2 for  $s_1$  and in Fig. 3 for  $s_2$ . Moreover, the corresponding mean ( $m$ ) and RMS ( $\sigma$ ) values of  $s_1$  and  $s_2$  are reported in Table 1. In each figure, the PDF of the real part, the imaginary part, the modulus and the phase (in degrees) of the echo are plotted in a specific subfigure. The mean value  $m$  is plotted in a dashed vertical line, and the mean value plus or minus the standard deviation  $\sigma$  are plotted in dotted vertical line. The PDF is fitted with a Gaussian PDF having the same parameters  $m$  and  $\sigma$  in full red line. Last, a comparison is made with the case of flat interfaces (whose PDF is a Dirac delta function) in green vertical line.

Concerning the first echo  $s_1$ , the imaginary part and the phase show a slight difference between the flat case and the mean value  $m_1$  of the rough case. Moreover, the dispersion around  $m_1$  is low: for instance, in the phase distribution, the RMS phase is  $< 1^\circ$  ( $0.275^\circ$ ). By contrast, a rather significant difference phase occurs in the real part and in the modulus. As expected, the (upper) surface roughness induces a decrease in the echo (real part or modulus) comparatively to the flat

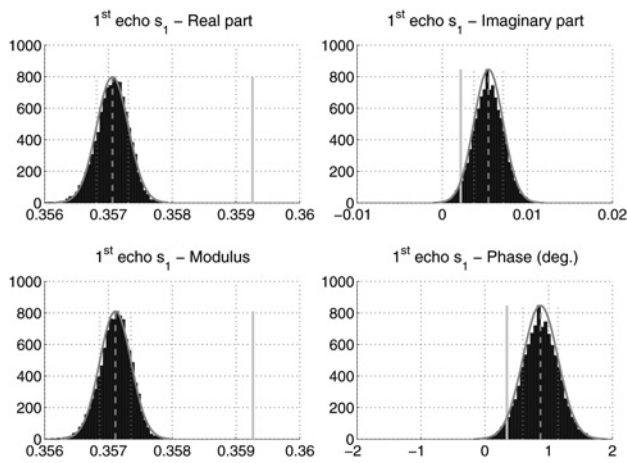


**Fig. 2** PDFs of the first echo  $s_1$  (real part, imaginary part, modulus and phase) obtained from 10 000 realisations, at a radar frequency  $f = 2$  GHz

Mean value is plotted in a dashed vertical line, and the mean value plus or minus the standard deviation are plotted in a dotted vertical line. Then, the PDF is fitted with a Gaussian PDF having the same statistical parameters (mean and RMS). A comparison is also made with the flat case in vertical line

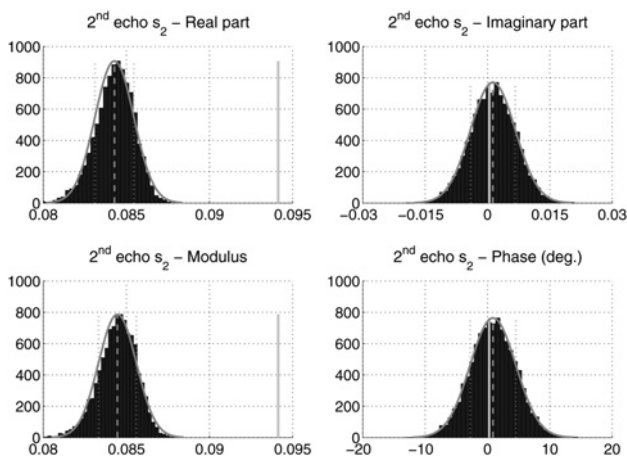


**Fig. 3** Same simulation parameters as in Fig. 2, but for the second echo  $s_2$ .

**Table 1** Mean ( $m$ ) and RMS ( $\sigma$ ) values of the two echoes  $s_1$  and  $s_2$  from Figs. 2 and 3, respectively: real part ( $\Re e$ ), imaginary part ( $\Im m$ ), modulus and phase (in degrees) components

|                 | $\Re e$ | $\Im m$ | Modulus | Phase, deg. |
|-----------------|---------|---------|---------|-------------|
| $s_1: m_1$      | 0.3571  | 0.0054  | 0.3571  | 0.873       |
| $s_1: \sigma_1$ | 0.0002  | 0.0017  | 0.0002  | 0.275       |
| $s_2: m_2$      | 0.0843  | 0.0013  | 0.0845  | 0.888       |
| $s_2: \sigma_2$ | 0.0012  | 0.0054  | 0.0011  | 3.663       |

case. However, this decrease remains small owing to the small electromagnetic roughness of the surface [evaluated by  $Ra_{r,1} = 0.042$ , see (3)] at this typical frequency. Moreover, the dispersion around  $m_1$  is low. It can be noticed that the general shape of the PDF resembles a Gaussian for the imaginary part and the phase, and also for the real part and the modulus.

The same qualitative observations can be made for the second echo  $s_2$ . Here, the relative differences between the flat case and the mean value  $m_2$  of the rough case are

higher, owing to the larger electromagnetic roughness of the layer:  $Ra_{r,2} = 0.181$  (which is close to the Fraunhofer limit, 0.196).

Second, in Fig. 4 the frequency behaviour of the echoes  $s_1$  and  $s_2$  (real part) is investigated in the whole range of the band  $f \in [0.5; 3.5]$  GHz, for which  $N = 1000$  Monte-Carlo processes were used.

As expected, for both echoes, the influence of the roughness of the interfaces continuously increases with frequency, inducing a broadening of the scattered beam around nadir and a decrease of the magnitude at nadir. This is confirmed by the Rayleigh roughness parameters  $Ra_{r,1}$  and  $Ra_{r,2}$  that increase as  $f$  increases. The decrease in modulus (or amplitude) is stronger for  $s_2$  than for  $s_1$  as predicted by  $Ra$  expressions. Then, the layer roughness cannot be neglected any longer for  $s_2$ , as it exceeds the Fraunhofer limit for  $f \gtrsim 2.17$  GHz.

Thus, within  $f \in [0.5; 3.5]$  GHz, the relative difference of the rough case with the flat case is weak for  $s_1$ , as it reaches only 0.5% for  $f = 1.5$  GHz, 1.3% for  $f = 2.5$  GHz, and 2.1% for  $f = 3.5$  GHz. Nevertheless, for  $s_2$ , this difference is more significant: it continuously increases with  $f$  from 6.5% for  $f = 1.5$  GHz to 19.8% for  $f = 3.5$  GHz. This confirms the qualitative Fraunhofer criterion given by (5), which is valid here only if  $f \lesssim 2.17$  GHz.

Finally, other simulations (not shown here) with a smaller antenna footprint (i.e. a narrower beamwidth) have been performed. As expected, a smaller antenna footprint induces an increased spatial variability of the echo amplitudes around their mean value, that is, an increased standard deviation.

In what follows, the echoes  $s_k(f)$  are denoted as  $s_k$  for the flat case and  $s_k w_k(f)$  for the rough case. Then, the term  $w_k(f)$  represents the frequency signature of the ratio of the rough case relatively to the flat case.

### 3 ESPRIT for TDE of radar data

In most cases, to provide the depth structure of the pavement from time delays associated with each layer and the wave

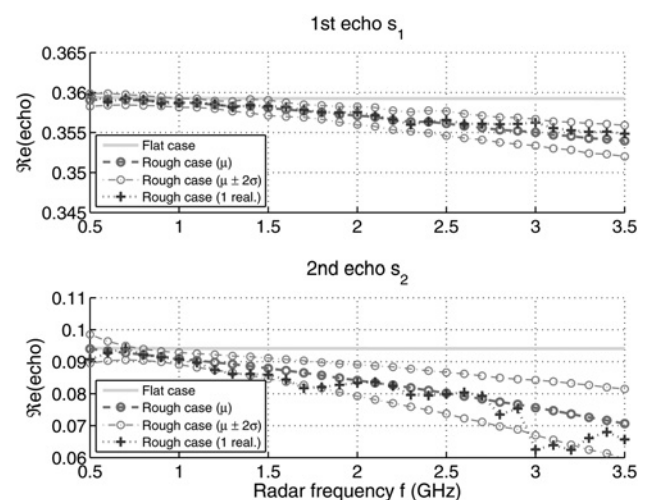


**Fig. 4** Frequency behaviour of the echoes  $s_1$  and  $s_2$  (real part) in the frequency band  $f \in [0.5; 3.5]$  GHz: comparison between the flat case, the mean value of the rough case and the mean value plus or minus twice the standard deviation of the rough case (from  $N = 1000$  realisations). The case of a particular realisation is also plotted for comparison

speed therein, radar data are processed on a scan-by-scan basis. Therefore the received signal is one dimensional and consists of the sum of  $K$  echoes of transmitted radar pulse. Within the scope of thin pavement survey, we focus on the signal processing techniques applicable for overlapping echoes within a limited bandwidth. Then, the algorithm ESPRIT [23, 24] has been selected for our purpose. As opposed to Section 2, it assumes a simplified data model to be presented hereafter. Then, this section recalls the principle of the algorithm and discusses practical considerations related to its use.

In far-field condition, impinging plane waves are reflected at each (rough) interface, and the received signal is then made up of  $K$  backscattered echoes (we concentrate here on  $K = 2$ , which corresponds to one layer with two rough interfaces). These echoes are simply time-shifted and attenuated copies of transmitted signal  $e(t)$  convoluted with the propagative channel response. An additive white Gaussian noise  $n(t)$  is assumed to represent the measurement uncertainties and the noise in the electronic devices. Most of the spectral analysis techniques applied to TDE process the data in the frequency domain [25]. The signal model is written as follows

$$\tilde{r}(f) = \sum_{k=1}^K s_k w_k(f) \tilde{e}(f) e^{-2j\pi f T_k} + \tilde{n}(f) \quad (7)$$

where the  $\tilde{\cdot}$  symbol represents the corresponding Fourier transform of temporal functions.  $s_k$  and  $s_k w_k(f)$  represent the  $k$ th ‘reflection coefficient’ (or rather echo) in the cases of flat and rough interfaces, respectively. The term  $w_k(f)$  represents the frequency behaviour of the  $k$ th echo for rough interfaces.

The ESPRIT algorithm has originally been proposed for array signal processing [23]. For TDE, the conventional ESPRIT algorithm considers an ideal data model, in which a flat surface and a lossless medium are assumed. This model has been used for the processing of radar data in far-field condition and for monostatic configuration (e.g. [21]). In this case, the term  $w_k(f) = 1$  in (7).

Considering  $N$  equispaced frequency samples  $f_n$  within the bandwidth  $B$ , the  $(N \times 1)$  received signal vector  $\tilde{r}$  can be written as follows [2]

$$\tilde{r} = \mathbf{A} \mathbf{s} + \tilde{\mathbf{n}} \quad (8)$$

where  $\mathbf{A}$  is the  $(N \times K)$  mode matrix, made up of the  $K$  steering vectors  $\mathbf{a}(T_k) = [e^{-2j\pi f_1 T_k}, e^{-2j\pi f_2 T_k}, \dots, e^{-2j\pi f_N T_k}]^T$  of size  $(N \times 1)$  as columns, with  $k \in \{1, 2, \dots, K\}$ ,  $\mathbf{A}$  is the  $(N \times N)$  diagonal matrix whose diagonal elements are the Fourier Transform  $\tilde{e}(f)$  of the radar pulse  $e(t)$ ,  $\mathbf{s}$  is the  $(K \times 1)$  vector of echoes amplitudes, that is, the Fresnel reflection coefficient from flat interfaces and lossless material at nadir, and  $\tilde{\mathbf{n}}$  is the  $(N \times 1)$  zero-mean noise vector with variance  $\sigma^2$ .

For TDE, the ESPRIT algorithm exploits an underlying rotational invariance between two adjacent data sub-bands. Considering two overlapping data sub-bands of  $N - 1$  samples each and overlapping with each other by  $N - 2$  samples, the associated  $(N - 1) \times K$ -dimensional mode matrices,  $\mathbf{A}_1$  and  $\mathbf{A}_2$ , are related to each other by the following  $(K \times K)$  diagonal matrix  $\Phi$ , whose elements

depend on the time delay to be estimated

$$\begin{aligned} \mathbf{A}_2 &= \mathbf{A}_1 \Phi, \quad \text{with} \\ \Phi &= \text{diag}(e^{-2j\pi\Delta/T_1}, \dots, e^{-2j\pi\Delta/T_K}) \end{aligned} \quad (9)$$

In practice,  $\Phi$  cannot be estimated from data. Nevertheless, on the basis of the eigendecomposition of the data covariance matrix  $\mathbf{I}_{\tilde{r}} = E[\tilde{r}\tilde{r}^H]$ , where  $E[\cdot]$  denotes the ensemble average, it can be shown that the diagonal elements of  $\Phi$  can be retrieved from the following similar matrix  $\Psi$  [24]

$$\Sigma_{o,2} \mathbf{V}_{\text{sig}} = (\mathbf{A}_2 \mathbf{A}_1^{-1} \Sigma_{o,1} \mathbf{V}_{\text{sig}}) \Psi \quad (10)$$

In the latter formula,  $\Sigma_{o,j}$  ( $j = 1, 2$ ) are two overlapping sub-band matrices of size  $(N - 1) \times N$ , which are defined as the  $N - 1$  upper and lower lines of the noise covariance matrix  $\Sigma_o$ , respectively, according to

$$\Sigma_o = \begin{pmatrix} - \\ \Sigma_{o,2} \end{pmatrix} = \begin{pmatrix} \Sigma_{o,1} \\ - \end{pmatrix} \quad (11)$$

$\mathbf{A}_j$  ( $j = 1, 2$ ) are two  $(N - 1) \times (N - 1)$  diagonal matrices defined from the pulse radar matrix  $\mathbf{A}$  as

$$\mathbf{A}_j = \text{diag}(\tilde{e}(f_j), \tilde{e}(f_{j+1}), \dots, \tilde{e}(f_{N-2+j})) \quad (12)$$

and  $\mathbf{V}_{\text{sig}}$  is made of the generalised eigenvectors of the signal subspace as columns. The time delays of the  $K$  echoes are retrieved from the arguments of the generalised eigenvalues of  $\Psi$ . Thus, ESPRIT requires to calculate the matrix  $\Psi$  in (10) with either the least-square method or the total least-square method [23].

ESPRIT can provide the time-delay estimates of the echoes when the covariance matrix of echoes has full rank. This condition is met when the echoes are not fully correlated. Further details on the estimation of the data covariance matrix are given in Section 4.

Algorithm implementation deserves a special attention within a multipath environment. As the source vector in the data model represents the different paths from the same source, the cross-correlation between echoes may be strong enough to perturb algorithm operations. Thus, the SSP (spatial smoothing process) or MSSP (modified spatial smoothing process) averaging technique is performed to alleviate the correlation influence. It requires a prior data whitening by the radar pulse shape  $\tilde{e}(f)$ . The frequency band ( $N$  data) is organised into  $M$  overlapping subbands of  $L$  data each, with  $L$  the effective bandwidth. For the largest overlapping ratio between sub-bands,  $L$ ,  $N$  and  $M$  are related to one another by  $N = L + M - 1$ . The frequency smoothing technique consists of averaging the  $M$  covariance matrices calculated from each sub-band vector ( $L$  data); its application is also called the forward technique (SSP) and the forward-backward technique (MSSP) if the data are averaged in the direct (as SSP) and the reverse orders simultaneously. Consequently, the covariance matrix to be processed by the sub-space algorithm is reduced to the size  $L \times L$ .

The optimum size of the sub-band was studied in the literature in order to approach the performance associated with null correlation. For pure cissoids in noise [2], the forward averaging SSP technique leads to a better time resolution when the effective frequency bandwidth lies between 50 and 70%. Performance is enhanced using the MSSP technique and

the optimum effective frequency bandwidth is between 80 and 90% of the total frequency bandwidth.

#### 4 Computer tests

In this section, the performance of the ESPRIT algorithm is tested on the data simulated from the PILE method in Section 2. By gradually taking account of the material conductivity and the layer roughness in the simulations, computer tests afford the sensitivity analysis on the TDE performance of the ESPRIT algorithm.

As a reminder, the layer thickness is  $\bar{H} = 20$  mm and the relative permittivities of the inner media  $\Omega_2$  and  $\Omega_3$  are  $\epsilon_{r2} = 4.5$  and  $\epsilon_{r3} = 7$ , respectively. The radar pulse  $e(t)$  is a Dirac pulse. The data vector is made of  $N = 31$  equally spaced frequency samples within  $[0.5; 3.5]$  GHz. The two echoes are slightly overlapped with the  $B\Delta\tau$  product equal to 0.85. The conductivity and the layer roughness introduce a dispersion within the backscattered signal that ESPRIT can only partly handle.

Thus, three data sets have been generated with PILE. Each one is made up of 1000 spatially independent snapshots at different SNR to be defined hereafter. The first data set matches the data model associated with the ESPRIT algorithm, that is, lossless media and flat interfaces. The second data set introduces a small conductivity within each layer ( $\sigma_2 = 5 \times 10^{-3}$  S/m and  $\sigma_3 = 10^{-2}$  S/m, respectively) that induces a small dispersion into the simulated signal. Finally, the third data set obeys the model in Section 2 with the latter small conductivity and the layer roughness accounted for.

Moreover, PILE provides the backscattered data vectors from each interface. Calling  $y_1(f)$  and  $y_2(f)$  the data vectors associated with the two interfaces, the data sets enable us to vary the cross-correlation amplitude between echoes. Like in [24], the high-correlation situation is obtained by running the algorithm from the covariance matrix  $\hat{\Gamma}_y^{hc}$  related to the sum  $y_1(f) + y_2(f)$ . By contrast, the best algorithm performance is obtained from the null correlation matrix  $\hat{\Gamma}_y^{nc}$ , which is calculated from the sum of the covariance matrices of the data related to the different data vectors. Both matrices are then defined as follows

$$\hat{\Gamma}_y^{hc} = \langle (y_1 + y_2) \times (y_1 + y_2)^H \rangle \quad (13)$$

$$\hat{\Gamma}_y^{nc} = \langle y_1 y_1^H \rangle + \langle y_2 y_2^H \rangle \quad (14)$$

The first situation is relevant to the experiment, because backscattered echoes originate from the same transmitter. To alleviate this problem, the covariance matrix is then estimated using the well-known SSP/MSSP averaging techniques as discussed in Section 3. The null correlation case allows us to get the best performance of the algorithm. Besides, it may help to select the best sub-band size for the SSP/MSSP averaging technique.

The SNR is defined as the ratio between the power of the strongest echo at the first frequency ( $f_1 = 0.5$  GHz) and the noise variance. The powers of the two sources are deduced from the particular realisation plotted in Fig. 4.

The performance of ESPRIT is assessed with a Monte-Carlo process of 500 independent runs of the algorithm, with independent noise snapshots. For each run, the ESPRIT method performs the TDE of the first two echoes  $\hat{T}_1$  and  $\hat{T}_2$ . Then, the layer thickness  $\hat{H}$  is estimated from

the knowledge of the dielectric constant  $\epsilon_{r2}$  inside  $\Omega_2$  with the relation [26]

$$\hat{H} \simeq \frac{c(\hat{T}_2 - \hat{T}_1)}{2\sqrt{\epsilon_{r2}}} \quad (15)$$

with  $c = 3 \times 10^8$  m/s the speed of light in vacuum.

The performance is assessed from the relative-root-mean-square error (RRMSE) of the layer thickness [2] as follows

$$\text{RRMSE}(H) = 100 \times \frac{\sqrt{(1/U) \sum_{j=1}^U (\hat{H}_j - H)^2}}{H} \quad (16)$$

where  $\hat{H}_j$  denotes the estimated thickness for the  $j$ th run of the algorithm, and  $H$  the true value.

Figs. 5 and 6 represent RRMSE variations on the estimated thickness ( $\hat{H}$ ) with respect to SNR for the three data sets. The best performance is obtained in dashed lines with the optim label, which corresponds to the ideal situation of both lossless layers (media) and flat surfaces along with null correlation between echoes [see (14)]. Then, the RRMSE continuously decreases with increasing SNR, which means that the TDE is unbiased.

When the conductivity is taken into account in the data set (Fig. 5), the best result is obtained for uncorrelated echoes (uncor label in the legend of the figure). The RRMSE

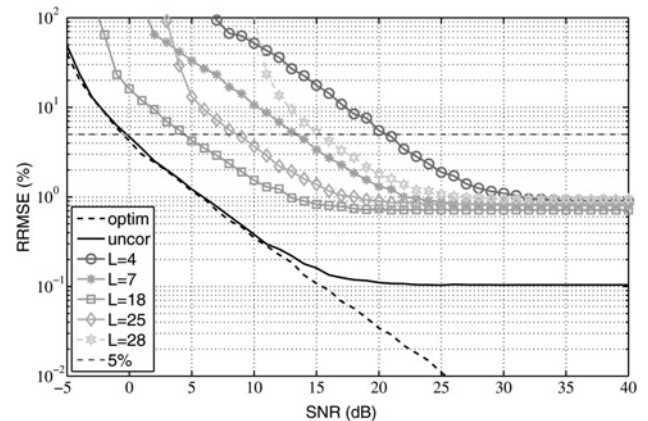


Fig. 5 RRMSE variations on the estimated thickness ( $\hat{H}$ ) against SNR for overlapping echoes, uncorrelated ('uncor') and correlated cases; for correlated case, the SSP method was used for various effective bandwidths  $L$ ,  $B = 3$  GHz (with  $B\Delta\tau = 0.84$ ), flat layer case

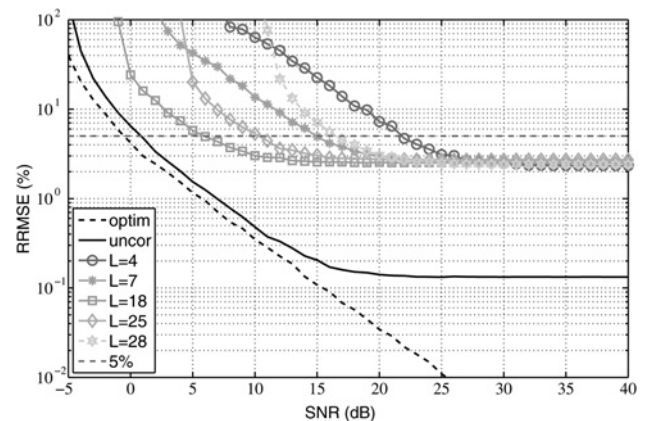


Fig. 6 Same parameters as in Fig. 5, but for the rough layer case

variations are the same as for the former ideal situation up to 12 dB SNR. Beyond this limit, the TDE method has a constant bias which is small enough compared to the accuracy requirement for pavement survey, that is, 5%. For the correlated case [see (13)], we used the SSP averaging technique with various effective bandwidths  $L$  as preprocessing. The results for different  $L$  reach the same asymptotic plateau of 1% in RRMSE at high SNR. Among the different cases,  $L = 18$  (corresponding to 58% in relative bandwidth) provides the closest result to the uncorrelated case.

In Fig. 6, the overall performance of the TDE algorithm degrades when both the conductivity and the layer roughness are taken into account. Compared to Fig. 5, the plateau is about 2.5 times larger and occurs at lower SNR. The plateau becomes closer to the 5% relative accuracy requirement in the practical situation of highly correlated echoes.

This sensitivity analysis shows that the simple data model associated with the conventional ESPRIT algorithm quickly departs from the data. Within the scope of pavement survey, the data model should include a damping factor whose magnitude is mostly dominated by the layer roughness.

## 5 Conclusions

This paper brought some evidence that the layer roughness has the most influence on deeper echoes compared to the surface echo. In particular, simulations showed that the spatial variations of the echo amplitudes are significant. Besides, the layer roughness provides a particular frequency signature of the amplitude of the echoes, that is, a decrease with respect to frequency. The difference with the flat situation is enhanced at higher frequencies, and especially for the second echo.

In the second part of the paper, the influence of conductivity and/or layer roughness on the inverse problem is shown, that is to say the thickness estimation by the selected TDE algorithm ESPRIT. Strictly speaking, the conductivity of the material must be taken into account in the algorithm: an asymptotic bias is revealed for average-to-high SNR. The bias magnitude is however small enough for the accuracy level required for pavement survey by GPR, that is, 5%. Taking the conductivity and the layer roughness into account, the performance of the TDE algorithm decreases with a relative error on the thickness that can be close to 2.5%.

It is believed that the use of a refined analytical data model (based on the Kirchhoff-tangent plane approximation [13, 15]) along with suitable modifications of the ESPRIT algorithm may greatly improve the performance for average-to-high SNR.

## 6 Acknowledgment

The authors would like to thank the anonymous reviewers for their relevant comments that helped improve the quality of the paper. The authors would also like to thank M.-T. Do, Ph. Côte, and X. Dérobert from the MACS (Monitoring, Assessment, Computational Sciences) department of IF STTAR (French institute of science and technology for transport) for their advice in the characteristics of the pavement structure.

## 7 References

- Lee, J., Nguyen, C., Scullion, T.: 'A novel, compact, low-cost, impulse ground-penetrating radar for nondestructive evaluation of pavements', *IEEE Trans. Instrum. Meas.*, 2004, **53**, pp. 1502–1509

- Bastard, C.L., Baltazart, V., Wang, Y., Saillard, J.: 'Thin-pavement thickness estimation using GPR with high-resolution and superresolution methods', *IEEE Trans. Geosci. Remote Sens.*, 2007, **45**, pp. 2511–2519
- Koudogbo, F., Mametsa, H., Combes, P.: 'Surface and volume scattering from natural and manmade rough surfaces in the process of setting up data base coefficients'. IEEE Int. Geoscience and Remote Sensing Symp., Piscataway, NJ, USA, 2003, vol. 7, pp. 4211–4213
- Lin, J., Liu, C., Li, J., Chen, X.: 'Measurement of concrete highway rough surface parameters by an X-band scatterometer', *IEEE Trans. Geosci. Remote Sens.*, 2004, **42**, pp. 1188–1196
- Koudogbo, F., Combes, P., Mametsa, H.-J.: 'Numerical and experimental validations of IEM for bistatic scattering from natural and manmade rough surfaces', *Prog. Electromagn. Res.*, 2004, **46**, pp. 203–244
- Déchamps, N., de Beaucoudrey, N., Bourlier, C., Toutain, S.: 'Fast numerical method for electromagnetic scattering by rough layered interfaces: propagation-inside-layer expansion method', *J. Opt. Soc. Am. A*, 2006, **23**, pp. 359–369
- Dérobert, X., Fauchard, C., Côte, P., et al.: 'Step-frequency radar applied on thin road layers', *J. Appl. Geophys.*, 2001, **47**, pp. 317–325
- Fauchard, C.: 'Utilisation de Radars très hautes fréquences: Application à l'auscultation non destructive des chaussées', PhD thesis, University of Nantes, France, 2001
- Wu, R., Li, X., Li, J.: 'Continuous pavement profiling with ground-penetrating radar', *Radar Sonar Navig.*, 2002, **149**, pp. 183–193
- Li, E., Sarabandi, K.: 'Low grazing incidence millimeter-wave scattering models and measurements for various road surfaces', *IEEE Trans. Antennas Propag.*, 1999, **47**, pp. 851–861
- Ogilvy, J.: 'Theory of wave scattering from random surfaces' (Institute of Physics Publishing, Bristol and Philadelphia, 1991)
- Ulaby, F., Moore, R., Fung, A.: 'Microwave remote sensing: active and passive', in: 'Radar remote sensing and surface scattering and emission theory', (Addison-Wesley, Advanced Book Program, Reading, Massachusetts, 1982, vol. 2)
- Pinel, N., Bourlier, C., Saillard, J.: 'Degree of roughness of rough layers: extensions of the Rayleigh roughness criterion and some applications', *Prog. Electromagn. Res. B*, 2010, **19**, pp. 41–63
- Yin, Z., Tan, H., Smith, F.: 'Determination of the optical constants of diamond films with a rough growth surface', *Diam. Relat. Mater.*, 1996, **5**, (12), pp. 1490–1496
- Pinel, N., Bourlier, C.: 'Scattering from very rough layers under the geometric optics approximation: further investigation', *J. Opt. Soc. Am. A*, 2008, **25**, pp. 1293–1306
- AFNOR Standard NF EN 13108-2: 'Bituminous mixtures – Material specifications – Part 2: Asphalt concrete for very thin layers', French standard, 2006
- Sarabandi, K., Li, E., Nashashibi, A.: 'Modeling and measurements of scattering from road surfaces at millimeter-wave frequencies', *IEEE Trans. Antennas Propag.*, 1997, **45**, pp. 1679–1688
- Adous, M., Queffelec, P., Laguerre, L.: 'Coaxial/cylindrical transition line for broadband permittivity measurement of civil engineering materials', *Meas. Sci. Technol.*, 2006, **17**, (8), pp. 2241–2246
- Lambot, S., Slob, E., van den Bosch, I., Stockbroeckx, B., Vanclooster, M.: 'Modeling of ground-penetrating radar for accurate characterization of subsurface electric properties', *IEEE Trans. Geosci. Remote Sens.*, 2004, **42**, pp. 2555–2568
- Liu, F.: 'Modélisation et Expérimentation Radar Impulsionnel et à Sauts de Fréquence Pour l'Auscultation de Milieux Stratifiés du Génie Civil', PhD thesis, University of Nantes, France, April 2007
- Thorsos, E., Jackson, D.: 'Studies of scattering theory using numerical methods', *Waves Random Media*, 1991, **1**, pp. 165–190
- Dusséaux, R., Oliveira, R.D.: 'Effect of the illumination length on the statistical distribution of the field scattered from one-dimensional random rough surfaces: analytical formulae derived from the small perturbation method', *Waves Random Complex Media*, 2007, **17**, pp. 305–320
- Roy, R., Kailath, T.: 'ESPRIT-estimation of signal parameters via rotational invariance techniques', *IEEE Trans. Acoust. Speech Signal Process.*, 1989, **37**, pp. 984–995
- Bastard, C.L., Baltazart, V., Wang, Y.: 'Modified ESPRIT (M-ESPRIT) algorithm for time delay estimation in both any noise and any radar pulse context by a GPR radar', *Signal Process.*, 2010, **90**, (1), pp. 173–179
- Shrestha, S., Arai, I.: 'Signal processing of ground penetrating radar using spectral estimation techniques to estimate the position of buried targets', *EURASIP J. Appl. Signal Process.*, 2003, **2003**, pp. 1198–1209
- Dérobert, X., Iaquina, J., Klysz, G., Balayssac, J.-P.: 'Use of capacitive and GPR techniques for the non-destructive evaluation of cover concrete', *NDT E Int.*, 2008, **41**, pp. 44–52